Journal of Power Sources 196 (2011) 4475–4482

Contents lists available at ScienceDirect

Journal of Power Sources

journal homepage: www.elsevier.com/locate/jpowsour

Factors affecting limiting current in solid oxide fuel cells or debunking the myth of anode diffusion polarization

Larry A. Chick[a,*], Kerry D. Meinhardt[a], Steve P. Simner[a,b,1], Brent W. Kirby[a], Mike R. Powell[a], Nathan L. Canfield[a]

[a] Pacific Northwest National Laboratory, Energy Materials, 904 Battelle Blvd., Richland, WA 99352, USA
[b] Savannah River Remediation, LLC, Savannah River Site, Aiken, SC 29808, USA

ARTICLE INFO

Article history:
Received 8 December 2010
Received in revised form
30 December 2010
Accepted 7 January 2011
Available online 19 January 2011

Keywords:
Solid oxide fuel cell
Limiting current
Diffusion polarization
Concentration polarization
Tortuosity
Button cell

ABSTRACT

Limiting current densities for solid oxide fuel cells were measured using both button cells and a flow-through cell. The cell anodes were supplied with mixtures of humidified hydrogen and various inert gasses. It was demonstrated that the true limiting current in flow-through cells is reached when either: the hydrogen is nearly or completely depleted at the anode-electrolyte interface near the outlet; or when the concentration of steam at that interface becomes high enough to interfere with adsorption or transport of the remaining hydrogen near the triple-phase boundaries. Choice of inert gas had no effect on limiting currents in the flow-through tests, indicating that diffusion within the porous anode had no significant effect on cell performance at high currents. In the button cells, the apparent limiting currents were significantly changed by the choice of inert gas, indicating that they were determined by diffusion through the bulk gas within the support tube. It was concluded that the apparent limiting currents measured in button cells are influenced more by parameters of the experimental setup, such as the proximity of the fuel tube outlet, than by the physical properties of the anode.

1. Introduction

Anode-supported, thin electrolyte solid oxide fuel cells (SOFCs) offer the advantage of moderate operating temperatures (650–800 °C) due to the low resistance of the thin (~10 μm) electrolyte. The moderate temperatures allow use of stainless steels for the frames, separator plates and manifolds, whereas the higher temperatures required to operate designs with thicker electrolytes require use of ceramics for these components.

It has been generally accepted [1–5] that the relatively thick (~0.5–1 mm) anode contributes significantly to performance loss due to anode diffusion polarization caused by sluggish diffusion of reactants into and/or products out of the pore structure of the anode.

Limiting current data taken from button cell experiments has often been used to infer properties of the anode that would account for sluggish mass transport. High pore tortuosity is commonly invoked to explain the button cell limiting current values. Anode tortuosities ranging from 4.5 up to 19 have been used to account for button cell data [2,3,6–8]. He et al. [5] performed diffusion experiments on an anode wafer using an oxygen pump and an oxygen sensor, and invoked a tortuosity factor of 21 to account for the data.

Yet most direct measurements conducted on anode materials indicate tortuosity values of less than 4. Fig. 1 shows the results of several studies. Williford et al. [9] conducted Wicke–Kallenbach diffusion experiments and found tortuosities ranging from 2.5 up to 4 for anode materials with porosities ranging from nearly 50%, down to 25%, respectively. They also conducted mercury porosimitry on the same samples and found tortuosities between about 2.5 and 3. Joshi et al. [10] performed lattice Boltzmann modeling of idealized anode structures. The line in Fig. 1 approximates the porosity–tortuosity trend derived from their Fig. 6. The tortuosity does not rise above 3 until the porosity decreases below 20%. Wilson et al. [11] performed focused ion beam-scanning electron microscopy to examine an actual anode material. They found a tortuosity of 2 at a porosity of 20%, although their sample volume was small, and might not represent the average anode properties. Drescher et al. [12] did permeation experiments and found a tortuosity of 2.7 at a porosity of 40%. Finally, Izzo et al. [13] used X-ray computed tomography and found an average tortuosity of 3.1 for a sample having 30% porosity.

A few researchers have explained button cell limiting current data without resorting to unrealistic tortuosities, but had to invoke other processes to rationalize the data. Williford [9] developed a surface diffusion-based model to explain button cell limiting cur-

* Corresponding author. Tel.: +1 509 375 2145; fax: +1 509 375 2186.
E-mail address: larry.chick@pnl.gov (L.A. Chick).
[1] Now at.

0378-7753/$ – see front matter © 2011 Elsevier B.V. All rights reserved.
doi:10.1016/j.jpowsour.2011.01.035

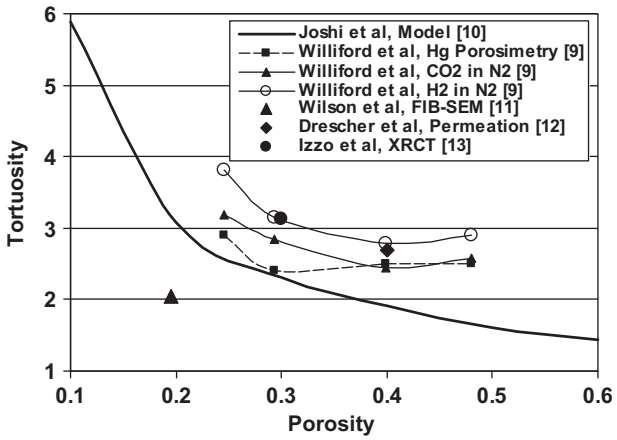

Fig. 1. Plot of relationship of tortuosity to porosity of SOFC anode materials determined by several means.

rents. Lee et al. [4] used a tortuosity of 3.5 for an anode with 35% porosity and explained the button cell data of Jaing and Virkar [3] by proposing a new model in which the rate-limiting reaction switches from the hydroxyl oxidation charge-transfer reaction to the hydrogen adsorption reaction near the limiting current density. Zhu et al. [14] also modeled the button cell data of Jaing and Virkar using 3.5 as the anode tortuosity. They scaled the exchange current densities in their electrochemical model to fit the limiting currents. DeCaluwe et al. [15] modeled button cell data of Zhao andVirkar [16] using reasonable tortuosity values, but in this case the limiting current used was for nearly pure (97%) hydrogen at high flow rates (300 sccm onto a 2 cm^2 active area). They also noted that it is reasonable to expect the tortuosity to be negatively correlated to porosity.

An explanation for the difficulties in accounting for button cell limiting currents solely based on anode processes begins to emerge in the work of Bessler [17] who performed modeling to investigate the effects of fuel inlet velocity and standoff distance on impedance spectra in button cell devices. He pointed out that diffusion in the bulk gas might dominate over convection. He also explained that, when hydrogen is the fuel, the creation of water at the interface causes a convective Stefan flow that moves away from the anode into the bulk gas. He stated, "Therefore, there will always be a region close to the anode where the convective flux is away from the surface and reactant transport to the anode is via diffusion against the flow only. At low gas inflow velocities, this region may be large. This additionally increases gas concentration resistance."

One objective of this paper is to present experimental evidence supporting Bessler's conclusions and to show that limiting current values obtained by button cell devices are dominated by diffusion in the bulk gas and not by diffusion through the porous anode. It will be demonstrated that the effect of anode diffusion on SOFC performance is much smaller than investigators have asserted when basing calculations on button cell data.

2. Experimental

Anode-supported cells were produced by standard organic tape casting, lamination and screen-printing techniques. Anode-electrolyte substrates were prepared by laminating NiO-YSZ anode tapes together with thin YSZ electrolyte tape. These were co-sintered at 1375 °C. A samarium doped ceria barrier layer was added by screen printing and firing at 1225 °C. Finally, the lanthanum strontium cobalt iron (LSCF) cathode was added by screen printing and firing at 1000 °C. After reduction the bulk anode was 550 μm thick, with solid phases composed of approximately 40% Ni and 60% YSZ by volume. The active anode was 10 μm thick, with solid phases composed of approximately 50% Ni and 50% YSZ. The post-sintered electrolyte was approximately 10 μm, the barrier layer 5 μm and the cathode 30–40 μm. Fabrication processes were slightly different between the flow-through and the button cells, and the resulting fraction porosity and pore sizes differed by about 20% (relative), as discussed in Section 3.1.

The anode-electrolyte supports for button cells were 25 mm diameter, with 19.5 mm diameter cathodes. The cathode area (3.0 cm^2) was used as the active cell area to calculate current densities. Screen-printed Pt grids with embedded Pt gauze and screen printed NiO grids with embedded Ni gauze were used as current collectors for the cathode and anode, respectively. The cells were sealed onto the ends of alumina tubes using Aremco cements. A photo of a mounted button cell is shown elsewhere [18]. Fig. 2 is a schematic of the button cell test fixture. Air was supplied to the cathode from a tube mounted within the furnace. Fuel was supplied to the anode from a 9.5 mm ID tube mounted within the tube to which the cell was fastened. This fuel tube had an adjustable stand-off distance, which was set at 1 or 2 or 4 cm.

The flow-through cell was a rectangle 14.5 cm × 9.8 cm. The cathode was 12.5 cm × 8.4 cm, giving an active area of 105 cm^2. The cell was glass sealed into a coated stainless steel frame, which was mounted in a furnace on a hearthplate that contained the gas manifolds. Fig. 3 is a photo of a cell mounted in a frame for the flow-through test apparatus. In this photo the cathode is facing up. The active area is the inner gray rectangle. Gas flow is from left to right, through the circular ports for the anode and through the triangular ports for the cathode. Fig. 4 is a schematic of the apparatus, in which both the cathode air and the anode fuel flow in the same direction (co-flow). The cathode cavity was 760 μm tall (from the surface of the cathode to the separator plate). The anode cavity was 380 μm tall. The gas flow cavities contained metallic meshes to facilitate current collection.

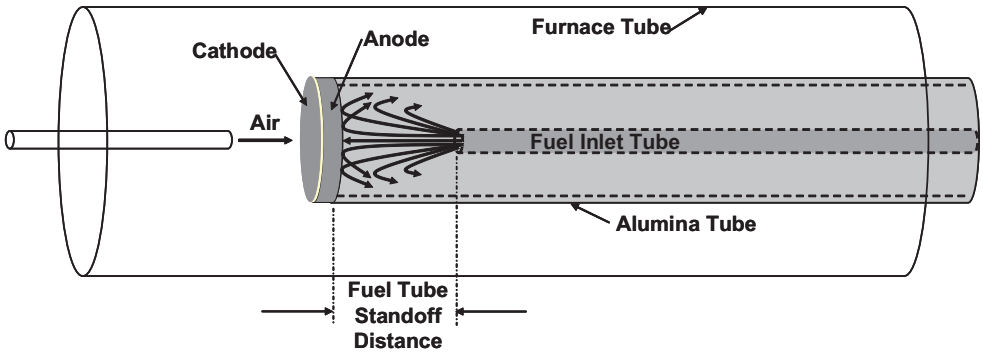

Fig. 2. Schematic of button cell test apparatus (not to scale).

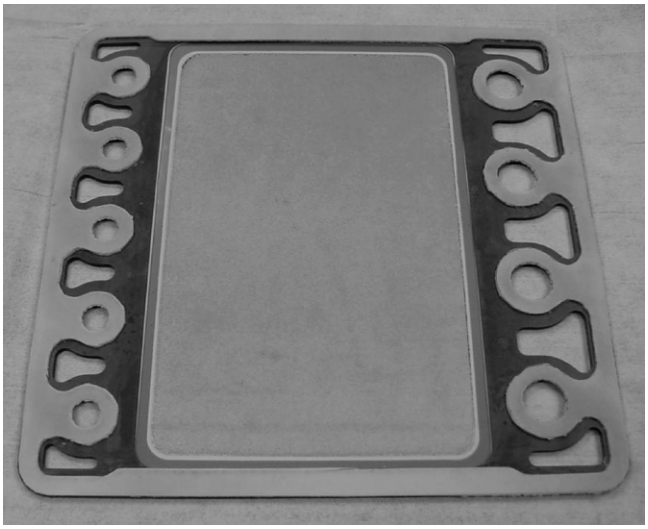

Fig. 3. Photo of cell mounted in frame for flow-through test apparatus. Cathode is facing up. Gas flow is from left to right.

For both button and flow-through experiments, anodes were supplied with hydrogen and an inert gas (He or N_2 or Ar) whose flow rates were regulated by mass flow controllers. The mixtures were bubbled through water at 25 °C, giving 3% steam by volume in the incoming anode gas. All quoted flow rates refer to dry gas values.

3. Results

3.1. Anode microstructure characterization

The top portion of Fig. 5 is a scanning electron micrograph of an epoxy-mounted, polished cross section of the bulk anode support structure of a button cell. Archimedes measurements established that the open porosity was 49%. The bottom portion of Fig. 5 shows the pores (black) selected using the image analysis software, ImageJ [19]. The objective was to get a measure of pore size appropriate to determine whether Knudsen diffusion is a significant diffusion mechanism in the microstructure. The procedure used to select these pores was first to filter the micrograph using the plugin filter, MultiThresholder. The Yen threshold was set at 108 and the image was despeckled once to yield an area fraction of pores of 49%, calibrated to the Archimedes measurements. Next the binary watershed process was used, which applied the fine white lines,

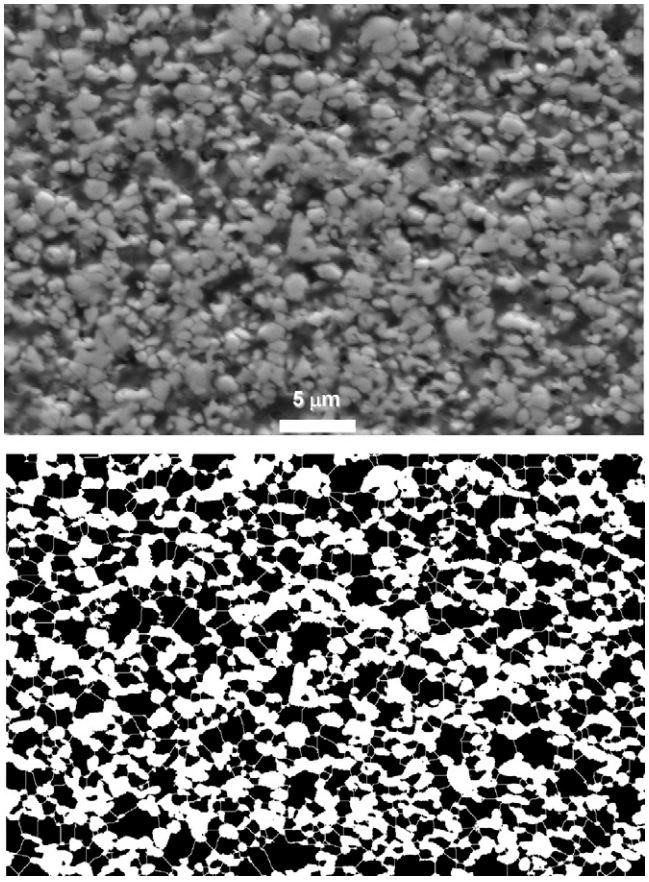

Fig. 5. Top: scanning electron micrograph of anode support microstructure of button cell, polished cross section. Bottom: filtered version of top microstructure, showing pores selected by ImageJ [19]. Porosity is 49%, average area-weighted pore radius is 0.8 µm.

breaking up the interconnected, complex shaped pores into more equiaxed shapes. Next the pores were analyzed, excluding the pores that overlapped the edges of the image. Included in the data on each pore were its area, maximum feret and minimum feret. The maximum feret, also known as the maximum caliper, is the maximum distance between any two points on the boundary of the pore. The minimum feret is the minimum distance between any two points on the boundary of the pore. For each pore, these two distances were averaged and taken as the pore diameter for the purpose of assessing diffusion. Furthermore, the overall average pore diameter

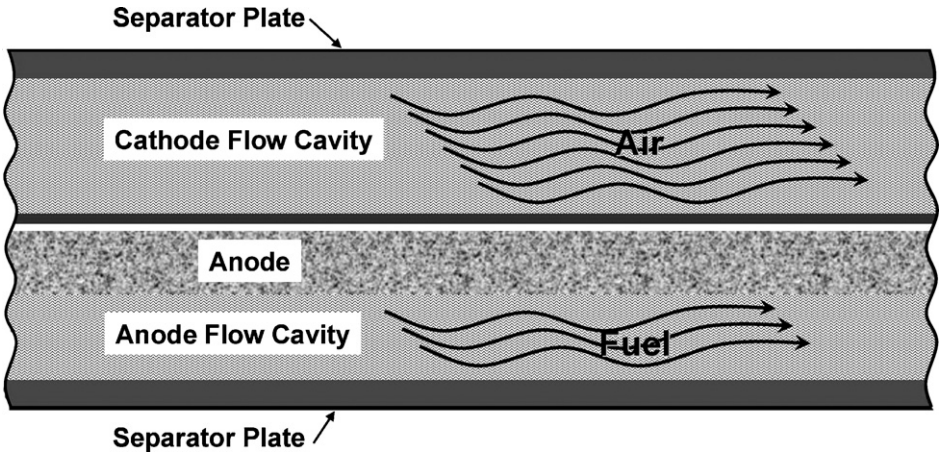

Fig. 4. Schematic of flow-through cell test apparatus (not to scale).

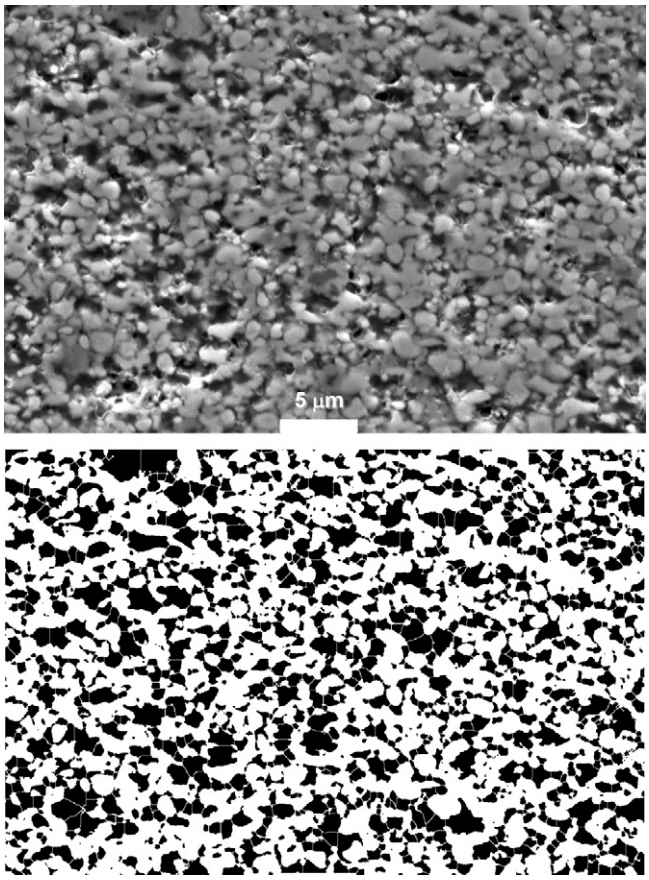

Fig. 6. Top: scanning electron micrograph of anode support microstructure of flow-through cell, polished cross section. Bottom: filtered version of top microstructure, showing pores selected by ImageJ [19]. Porosity is 38%, average area-weighted pore radius is 0.6 μm.

was taken as the area-weighted (not the number weighted) average of the individual pore diameters. The area-weighted average was used because it was reasoned that more gas molecules diffuse through larger than through smaller pores. Thus, the area-weighted average pore radius is a reasonable measure of the distance the "average" molecule must travel to collide with a pore wall. For the button cell anode microstructure shown in Fig. 5, the area-weighted average pore radius is 0.8 μm.

The top portion of Fig. 6 is a scanning electron micrograph of the anode support structure of a flow-through cell. Archimedes measurements established that the open porosity is 38%. The bottom portion of Fig. 6 shows the pores selected using the procedure described above. The Yen threshold was set to 133 in order to yield 38% pore area. In this case the area-weighted average pore radius is 0.6 μm.

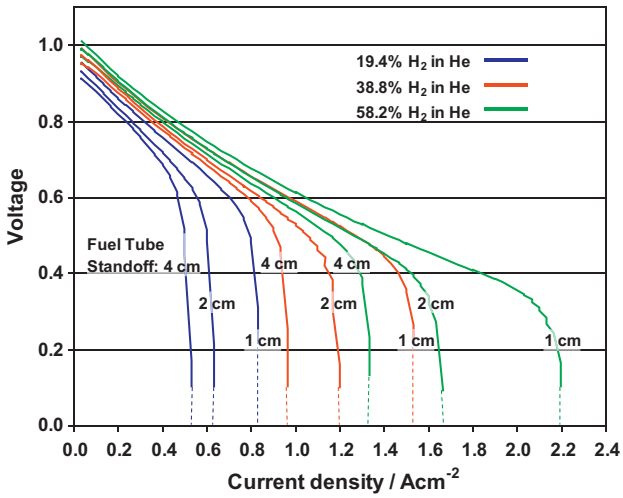

Fig. 7. Button cell data for three concentrations of hydrogen with 3% water in helium with three different fuel supply tube standoff distances. Total anode gas flow rate was 200 sccm. Limiting currents were estimated by extrapolating the *I–V* data (broken lines).

The active anode microstructures contain somewhat less porosity than the bulk anodes. For the button and flow-through cells, the active anode porosities, measured using ImageJ with the same filter thresholds used for the bulk, were 40% and 35%, respectively.

3.2. Button cell data

Fig. 7 shows cell voltage versus current density (*I–V*) curves for button cell tests at 750 °C. Curves for three hydrogen concentrations and three fuel tube standoff distances are shown. Total anode flow rate was always 200 standard cubic centimeters per minute (sccm). The curves were extrapolated to zero voltage to estimate the limiting currents.

Table 1 lists measured and derived data from the set of *I–V* curves plotted in Fig. 7. The estimated limiting current density is listed in the third column. Fuel (H_2) utilization at the limiting current density is shown in the fourth column. Based on the fuel utilization and the inlet gas composition, the concentration of hydrogen and water at the outlet were calculated and are listed in the fifth and sixth columns. The highest limiting current, 2.2 A cm^{-2}, occurred with the highest hydrogen concentration with the shortest standoff distance. The lowest hydrogen concentration with the longest standoff distance gave the lowest limiting current, 0.53 A cm^{-2}.

The button cell *I–V* curves in Fig. 8 were taken at 800 °C, with 200 sccm total anode gas flow rate. Hydrogen concentrations were either 24.3% or 48.5%. For each concentration, the test with argon as the carrier gas had significantly lower limiting current than the test with helium as the carrier gas.

Table 1
Button cell test parameters and results.

Percent H_2 at inlet	Standoff distance (cm)	Limiting current density (A cm^{-2})	H_2 utilization	H_2 at outlet	H_2O at outlet
19.40%	1	0.83	43.5%	11.0%	11.4%
38.80%	1	1.53	40.0%	23.3%	18.5%
58.20%	1	2.20	38.3%	35.9%	25.3%
19.40%	2	0.63	33.1%	13.0%	9.4%
38.80%	2	1.20	31.3%	26.6%	15.2%
58.20%	2	1.67	29.1%	41.3%	19.9%
19.40%	4	0.53	27.8%	14.0%	8.4%
38.80%	4	0.97	25.2%	29.0%	12.8%
58.20%	4	1.33	23.2%	44.7%	16.5%

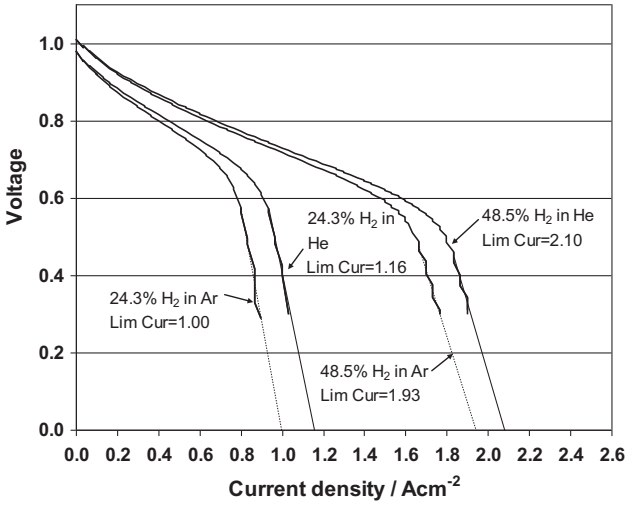

Fig. 8. Button cell data taken at 800 °C, all at 200 sccm flow rate with 1 cm standoff distance. Limiting current densities ("Lim Cur") were estimated by extrapolation to zero volts.

3.3. Flow-through cell data

Figs. 9–11 are *I–V* curves taken at 750 °C in the flow-through apparatus at hydrogen concentrations of 15%, 46% and 97%, respectively. The tests at the lower hydrogen concentrations (Figs. 9 and 10) used nitrogen as the carrier gas. In each case, total anode flow rates were varied to give a range of limiting currents. Limiting currents were estimated by extrapolating to zero volts.

Table 2 lists measured and derived data from the set of *I–V* curves plotted in Figs. 9–11. The estimated limiting current density is listed in the third column. Fuel (H_2) utilization at the limiting current density is shown in the fourth column. Based on the fuel utilization and the inlet gas composition, the concentration of hydrogen and water at the outlet of the flow-through cell were calculated and are listed in the fifth and sixth columns.

Fig. 12 is a plot of *I–V* curves taken at 750 °C in the flow-through apparatus at a hydrogen concentration of 15%. Flow rates were varied from 1450 sccm up to 8320 sccm to give a range of limiting currents. Two sets of tests were run, one set with argon as the carrier gas ("*X*"s) and one set with helium as the carrier gas (diamonds). The two sets of *I–V* curves are nearly identical with very slightly higher limiting currents for the helium carrier gas at the two highest flow rates.

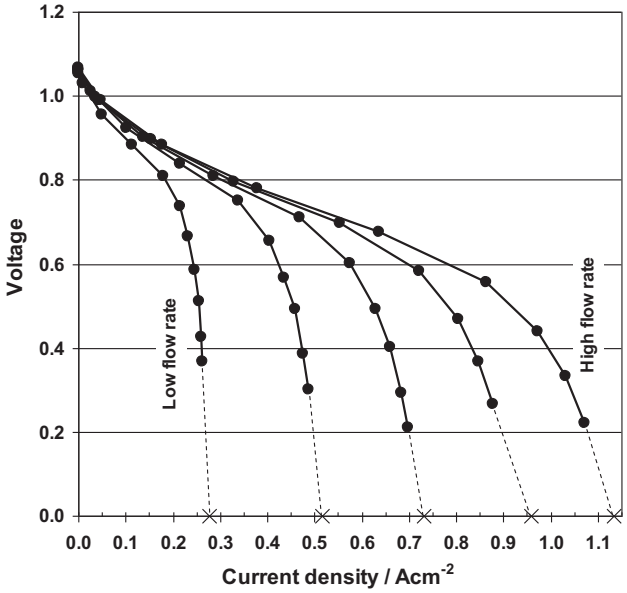

Fig. 10. Flow-through cell data for approximately 47% hydrogen with 3% water in nitrogen at 750 °C. Anode flow rates ranged from 449 to 1978 sccm. "*X*"s are limiting currents estimated by extrapolating the *I–V* data.

3.4. Comparison of button cell to flow-through cell results

Fig. 13 is a plot including both the button cell data from Fig. 7 and Table 1 and the flow-through data from Figs. 9–11 and Table 2. The limiting current values are plotted as functions of the specific hydrogen flow rate in sccm per cm^2 of active area. The black, broken lines show where the limiting currents would fall if they occurred at 20%, 50%, or 100% hydrogen utilization. The limiting currents for all

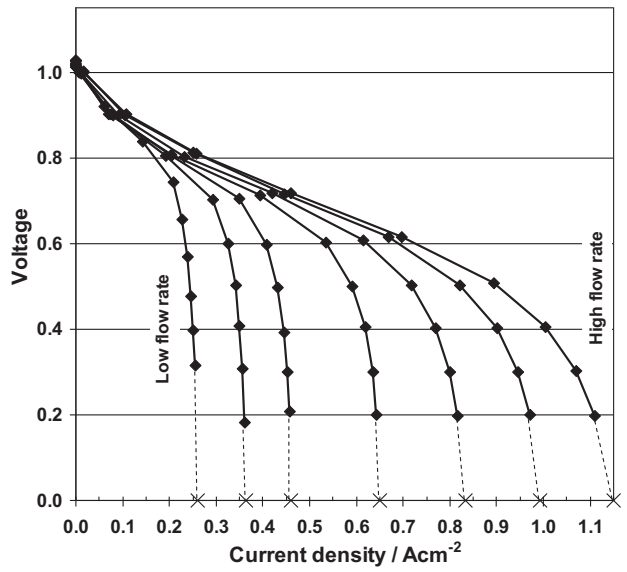

Fig. 9. Flow-through cell data for approximately 15% hydrogen with 3% water in nitrogen at 750 °C. Anode flow rates ranged from 1343 to 7408 sccm. "*X*"s are limiting currents estimated by extrapolating the *I–V* data.

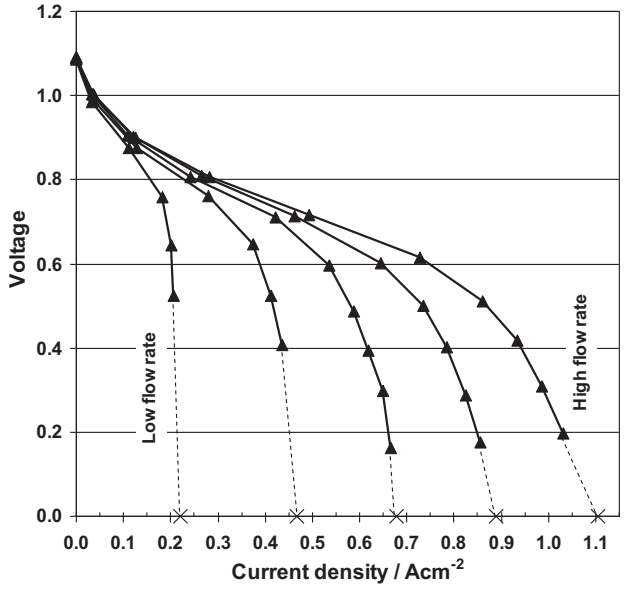

Fig. 11. Flow-through cell data for 97% hydrogen with 3% water at 750 °C. Anode flow rates ranged from 207 to 964 sccm. "*X*"s are limiting currents estimated by extrapolating the *I–V* data.

Table 2
Flow-through cell test parameters and results.

Percent H_2 at inlet	Inlet flow rate (sccm)	Limiting current density (Acm^{-2})	H_2 utilization	H_2 at outlet	H_2O at outlet
14.9%	1343	0.261	93.3%	1.0%	16.9%
14.8%	1984	0.364	88.9%	1.6%	16.1%
14.7%	2618	0.460	85.4%	2.2%	15.6%
14.8%	3849	0.651	81.8%	2.7%	15.1%
14.9%	5058	0.832	79.1%	3.1%	14.8%
15.0%	6247	0.992	76.0%	3.6%	14.4%
15.1%	7408	1.149	73.6%	4.0%	14.1%
44.8%	449	0.278	98.9%	0.5%	47.3%
46.3%	834	0.517	95.9%	1.9%	47.4%
46.9%	1217	0.732	91.9%	3.8%	46.1%
47.1%	1599	0.959	91.2%	4.1%	46.0%
47.3%	1978	1.133	86.7%	6.3%	44.0%
97.0%	207	0.220	78.3%	21.1%	78.9%
97.0%	397	0.468	87.1%	12.6%	87.4%
97.0%	587	0.678	85.3%	14.3%	85.7%
97.0%	775	0.890	84.8%	14.8%	85.2%
97.0%	964	1.105	84.6%	14.9%	85.1%

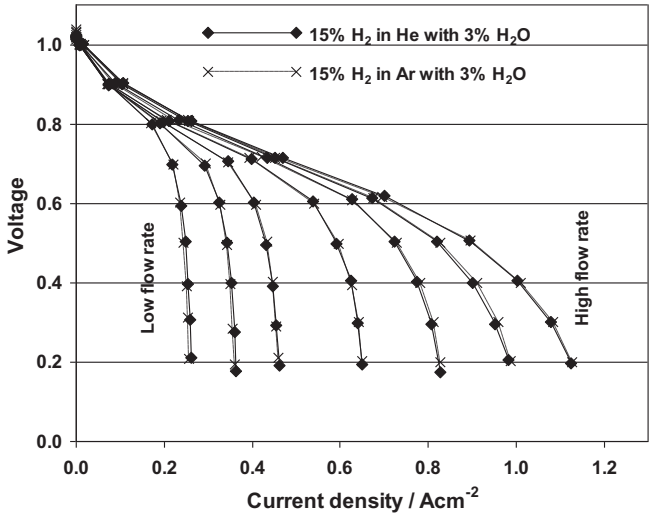

Fig. 12. Flow-through cell *I–V* curves for 15% hydrogen with 3% water, with balance either helium or argon, 750 °C. Anode flow rates ranged from 1450 to 8320 sccm.

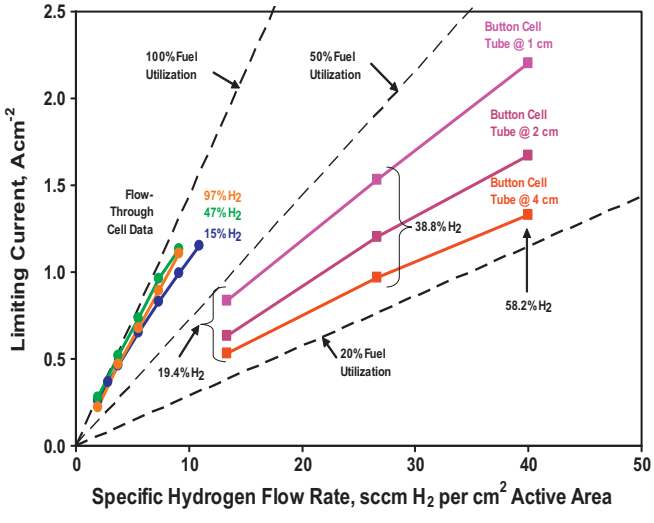

Fig. 13. Button cell and flow-through cell data with estimated limiting currents plotted as functions of specific hydrogen flow rate.

of the button cell tests fall below 50% fuel utilization. In contrast, those for the flow-through cell all fall well above 50% hydrogen utilization, with some very near 100%. Furthermore, the limiting currents for the button cells are strongly dependent on the fuel tube standoff distance.

4. Discussion

Based on the Stefan–Maxwell equation, Jiang and Virkar [3] derived the following equation for the diffusion coefficient for hydrogen, D_{H_2}, in the porous anode for the ternary system, H_2–H_2O–inert when the cell is running at steady state:

$$\frac{1}{D_{H_2}} = \frac{1}{D_{K,H_2}} + \frac{X_{inert}}{D_{H_2,inert}} + \frac{1 - X_{inert}}{D_{H_2,H_2O}} \quad (1)$$

where D_{K,H_2} is the Knudsen diffusion coefficient for hydrogen, $D_{H_2,inert}$ is the binary diffusion coefficient for hydrogen in an inert carrier gas, D_{H_2,H_2O} is the binary diffusion coefficient for hydrogen in steam, and X_{inert} is the mole fraction of the inert gas. Note that D_{H_2} will not vary while steam replaces hydrogen as the anode gas progresses over the flow-through cell, because it depends only on the concentration of the inert carrier gas, which remains constant across the cell.

The Knudsen diffusion coefficient, $D_{K,n}$ for species, n, is given by [20]:

$$D_{K,n} = 4850d\left(\frac{T}{M_n}\right)^{1/2} \quad (2)$$

where $D_{K,n}$ has units of $cm^2\ s^{-1}$, d is the pore diameter in centimeters, T is the temperature in Kelvins, and M_n is the molecular weight of n.

The binary diffusion coefficient, D_{m-n} for species m in n is given by [21]:

$$D_{m-n} = \frac{T^{1.75}(1/M_m + 1/M_n)^{1/2}}{1000p[(v_m)^{1/3} + (v_n)^{1/3}]^2} \quad (3)$$

where p is the pressure in atmospheres and v_m is the diffusion volume of species, m.

The effective diffusion coefficient [3], which actually governs the flux of hydrogen within the porous anode, is given by:

$$D_{H_2,eff} = D_{H_2}\frac{V_p}{\tau} \quad (4)$$

where V_p is the volume fraction porosity and τ is the tortuosity.

If the pores within the anode are small enough, molecules will be more likely to collide with a pore wall than with another molecule.

Table 3
Experimental conditions and diffusion coefficients for the tests plotted in Figs. 8 and 12.

Fig.	T (°C)	Pore radius (μm)	V_p	Inert gas	Mole fraction inert	D_{K,H_2}	$D_{H_2,inert}$	D_{H_2,H_2O}	D_{H_2}	$D_{H_2,eff}$
8	800	0.80	0.49	He	0.485	18.0	15.6	8.3	4.2	0.82
8	800	0.80	0.49	Ar	0.485	18.0	7.4	8.3	3.2	0.63
8	800	0.80	0.49	He	0.727	18.0	15.6	8.3	4.2	0.82
8	800	0.80	0.49	Ar	0.727	18.0	7.4	8.3	3.2	0.63
12	750	0.60	0.38	He	0.820	13.2	14.3	7.6	3.6	0.55
12	750	0.60	0.38	Ar	0.820	13.2	6.8	7.6	2.8	0.43

In that case, Knudsen diffusion will be the dominant diffusion mechanism. If Knudsen diffusion dominates, the choice of inert carrier gas should have little effect on the rate of hydrogen diffusion. However, if the pores are large enough that binary diffusion is important, then the diffusion rate of hydrogen will be affected by the choice of inert carrier gas (He versus Ar), through the binary coefficient, $D_{H_2,inert}$, because collisions occur more often with other molecules than with pore walls. The diffusion coefficients are listed in Table 3. Based on the data in Fig. 1, a tortuosity of 2.5 was used in each case to calculate $D_{H_2,eff}$.

In each of the three cases where only the choice of inert carrier gas was changed (top pair, middle pair and bottom pair in Table 3), the effective diffusion coefficient for helium was about 30% higher than for argon. Therefore, if diffusion through the pores in the anode was a significant factor in determining the limiting current in the flow-through cell, one would expect to find a significant difference between the limiting currents measured with He versus Ar as the inert carrier gas. There is no such difference, as shown in Fig. 12. Furthermore, if diffusion through the anode porosity was not a factor in the flow-through cell, one would not expect it to be a factor in the button cells since the button cell anode had even more and larger porosity than the flow through cell and was the same thickness. Yet it is evident (Fig. 8) that the choice of inert gas does affect the limiting current measured in button cells.

The explanation is that in button cells the limiting current is affected by binary diffusion (Eq. (3)) through bulk, stagnant gas adjacent to the anode within the alumina tube on which the cell is mounted. This accounts for the effect of inert gas choice in Fig. 8 and for the lower attainable fuel utilizations for the button cell tests in Fig. 13. Jiang and Virkar [3] also found that the choice of inert carrier gas affected the limiting current in their button cell tests.

On the other hand, the limiting currents derived from the flow-through tests are determined by depleting the hydrogen at the anode-electrolyte interface, or by building up enough water at the interface to block access to the remaining hydrogen.

Fig. 14 is a plot of percent hydrogen remaining in the outlet gas versus the limiting current density for the flow-through tests with 15% and 47% hydrogen at the inlet (Figs. 9 and 10 and Table 2). These trends show that the amount of hydrogen swept out of the cell without being utilized increases as the limiting current (and the gas flow rate) increases. It is not surprising that some hydrogen is swept out of the cell in the convective flow before being able to diffuse to the anode-electrolyte interface. For the data shown in Fig. 9, anode flow velocities are quite high, ranging from 137 cms^{-1} to 769 cms^{-1}. Residence time over the active area of the cell was from 0.013 to 0.079 s.

For the flow-through tests with 97% hydrogen at the inlet, there was still between 13% and 21% hydrogen available to the anode near the outlet when the cell reached the limiting current. However, under these conditions, the steam concentration at the outlet was very high, ranging from 79% to 87%. There may be an equilibrium between water in the gas phase and adsorbed hydroxyl groups on the surface, which block hydrogen adsorption. Upon changing from higher to lower incoming steam concentrations the

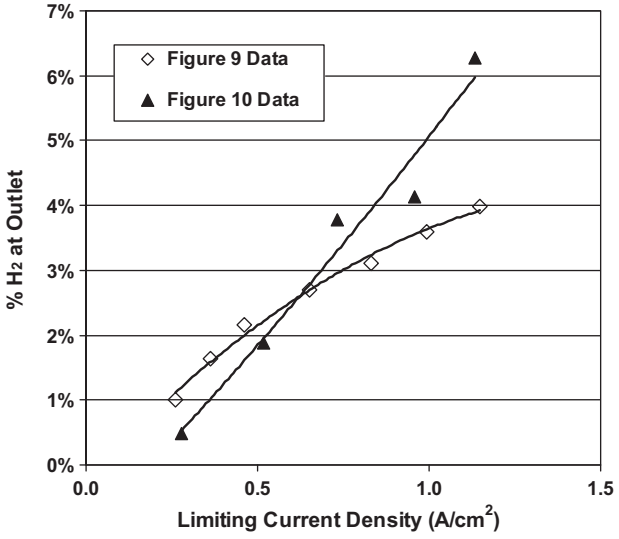

Fig. 14. Hydrogen remaining at the flow-through cell outlet plotted versus limiting current for the *I–V* curves in Fig. 9 (open diamonds, 15% H_2, 3% H_2O in N_2) and 10 (filled triangles, 47% H_2, 3% H_2O in N_2).

OCV has been observed to rise much more slowly than a purely diffusive process would predict, further supporting a slow desorption process.

It is evident that much of the fuel never got close enough to the anode to be consumed in the button cell apparatus. The apparent limiting current density was reached when the fuel near the surface of the anode was nearly depleted, as in the flow-through cell. However, while the surface fuel depletion in the flow-through cell was a result of bulk depletion of the hydrogen in the gas, in the button cell the fuel became locally depleted at the anode surface due to its having to diffuse through a column of gas that was stagnant or moving *away* from the anode [17]. Given a certain hydrogen concentration in the incoming fuel gas mixture, the limiting current in the button cell apparatus is determined by the fuel tube standoff distance and the diffusion coefficient for hydrogen in the carrier gas. Placing the fuel tube outlet closer to the anode forces more fresh fuel near the anode, thus increasing the apparent limiting current. However, even at the closest fuel tube position, the overall fuel utilization was always below 45% (Fig. 13).

A similar bulk diffusion phenomenon accounts for the results reported by He et al. [5]. They erected a device consisting of a 9.9 cm in tube with an oxygen pump at one end and a porous Ni-YSZ disc at the other. They then pumped oxygen into the tube at a controlled rate and measured the Nernst potential at an intermediate location along the tube. When the Nernst potential reached steady state, they calculated the hydrogen concentration, noted the oxygen flux and performed diffusion calculations that were limited to diffusion through the porous disk. Their implicit assumption was that the tube acted like a "stirred tank reactor". In other words, that there were no concentration gradients along the length of the tube. This accounts for their having to invoke a tortuosity factor of 21 to

explain the data based solely on diffusion rates through the porous disk.

Zhu et al. [14] explicitly invoked the stirred tank assumption in modeling button cell data of Jiang and Virkar [3]. Although they did not resort to an unusually high tortuosity factor to explain the data, they used button cell limiting current density data to scale exchange current densities. The results presented here clearly demonstrate that the stirred tank assumption is invalid for button cell tests.

5. Conclusions

In the cells tested, the process of diffusion of hydrogen through the pores of the anode did not significantly contribute to the limiting current. Flow-through cell tests indicate that the limiting current is reached when either the hydrogen is nearly or completely depleted at the anode-electrolyte interface near the outlet or when the concentration of steam at that interface becomes high enough to interfere with adsorption or transport of the remaining hydrogen at the triple-phase boundaries. Button cell data should not be used to infer properties of the anode affecting diffusion, such as pore tortuosity, because the apparent limiting currents measured in these devices are determined more by parameters of the experimental setup, such as the proximity of the fuel tube outlet, than by the physical properties of the anode. There is no significant polarization loss associated with diffusion of fuel through the porous anode in typical anode supported SOFCs.

References

[1] S.C. Singhal, K. Kendall, High Temperature Solid Oxide Fuel Cells Fundamentals, Design and Applications, Elsevier, Oxford, 2004.
[2] J.W. Kim, A.V. Virkar, K.Z. Fung, K. Mehta, S.C. Singhal, J. Electrochem. Soc. 146 (1) (1999) 69–78.
[3] Y. Jiang, A.V. Virkar, J. Electrochem. Soc. 150 (7) (2003) A942–A951.
[4] W.Y. Lee, D. Wee, A.F. Ghoniem, J. Power Sources 186 (2009) 417–427.
[5] W. He, K.J. Yoon, R.S. Eriksen, S. Gopalan, S.N. Basu, U.B. Pal, J. Power Sources 195 (2010) 532–535.
[6] S.H. Chan, K.A. Khor, Z.T. Xia, J. Power Sources 93 (2001) 130–140.
[7] K.J. Yoon, S. Gopalan, U.B. Pal, J. Electrochem. Soc. 156 (3) (2009) B311–B317.
[8] H. Zhu, R.J. Kee, J. Electrochem. Soc. 153 (9) (2006) A1765–A1772.
[9] R.E. Williford, L.A. Chick, G.D. Maupin, S.P. Simner, J.W. Stevenson, J. Electrochem. Soc. 158 (8) (2003) A1067–A1072.
[10] A.S. Joshi, K.N. Grew, J.R. Izzo Jr., A.A. Peracchio, W.K.S. Chiu, J. Fuel Cell Technol. 7 (1) (2010) 011006-1–-111006.
[11] J.R. Wilson, W. Kobsiriphat, R. Mendoza, H.Y. Chen, J.M. Hiller, D.J. Miller, K. Thornton, P.W. Voorhees, S.B. Adler, S.A. Barnett, Nat. Mater. 5 (2006) 541–544.
[12] I. Drescher, W. Lehnert, J. Meusinger, Electrochim. Acta 43 (19–20) (1998) 3059–3068.
[13] J.R. Izzo Jr., A.S. Joshi, K.N. Grew, S. Chiu, A. Tkachuk, S. Wang, W. Yun, J. Electrochem. Soc. 155 (5) (2008) B504–B508.
[14] H. Zhu, R.J. Kee, V.M. Janardhanan, O. Deutschmann, D.G. Goodwin, J. Electrochem. Soc. 152 (12) (2005) A2427–A2440.
[15] S.C. DeCaluwe, H. Zhu, R.J. Kee, G.S. Jackson, J. Electrochem. Soc. 155 (6) (2008) B538–B546.
[16] F. Zhao, A.V. Virkar, J. Power Sources 141 (2005) 79–95.
[17] W.G. Bessler, J. Electrochem. Soc. 153 (8) (2006) A1492–A1504.
[18] S.P. Simner, J.F. bonnet, N.L. Canfield, K.D. Meinhardt, J.P. Shelton, V.L. Sprenkle, J.W. Stevenson, J. Power Sources 113 (2003) 1–10.
[19] W.S. Rasband, U.S. National Institutes of Health, Bethesda, Maryland, http://rsb.info.nih.gov/ij/ (1997–2009).
[20] E.L. Cussler, Diffusion: Mass Transfer in Fluid Systems, second ed., Cambridge University Press, New York, 1997.
[21] E.N. Fuller, P.D. Schettler, J.C. Giddings, Ind. Eng. Chem. 58 (5) (1966) 18–27.